PHYSICAL REVIEW B **89**, 024306 (2014)

Quantitative macroscopic treatment of the spatiotemporal properties of spin crossover solids based on a reaction diffusion equation

Miguel Paez-Espejo, Mouhamadou Sy, François Varret, and Kamel Boukheddaden[*]
Groupe d'Etudes de la Matière Condensée, UMR 8635, CNRS-Université de Versailles Saint-Quentin-en-Yvelines,
45 Avenue des Etats Unis, F-78035 Versailles, France

(Received 3 August 2013; revised manuscript received 3 January 2014; published 28 January 2014)

We propose here a new theoretical treatment of the spatiotemporal properties in spin-crosser solids, based on the expansion of the free energy taking into account the spatial fluctuations of the high-spin (HS) fraction. This leads to an equation of motion on the HS fraction following a reaction diffusion equation (RDE), in which most of the parameters can be derived from the experiments. This equation involves the true temporal and spatial scales at variance from the previous stochastic microscopic models, which were based on a homogeneous treatment of the crystal's properties. We have illustrated this new treatment for a two-dimensional rectangularly shaped system with a square symmetry and we could reproduce quantitatively the process of nucleation, growth, and propagation of the HS fraction inside the thermal hysteresis loop, accompanying a first-order transition. The computed spatiotemporal evolution of the system allowed one to follow the propagation of a well-defined macroscopic HS:LS interface, which was found in excellent quantitative agreement with the experimental observations of optical microscopy on the switchable spin crossover crystal [$\{\mathrm{Fe(NCSe)(py)_2}\}_2$($m$-bpypz)]. The RDE treatment should generate predictive models for novel spatiotemporal effects in spin crossover solids and more generally for all kinds of switchable molecular solids.

DOI: 10.1103/PhysRevB.89.024306 PACS number(s): 75.30.Wx, 68.35.Rh, 64.60.De

I. INTRODUCTION

The high-spin (HS)↔ low-spin (LS) transition [1] is still the object of various experimental and theoretical investigations. The interplay between the spin crossover and the structural properties, originating from intramolecular vibronic coupling, can be enhanced by elastic intermolecular interactions. The contributions of long-range elastic interactions, particularly at the solid state, lead to rather abrupt thermal spin transition and in many cases to hysteresis behavior denoting a first-order phase transition or two-step spin transition [2–4]. However, a gradual transition, corresponding to the simple Boltzmann distribution between two states, is generally obtained in highly diluted crystals (i.e., noncooperative systems). The molecular spin state transition from LS to HS is accompanied by an expansion of the unit cell of the crystal owing to a stretching of the bond lengths (∼10% for the $\mathrm{Fe^{II}}$ ion). Extensive research efforts have been devoted to the observation and/or the visualization of the spatiotemporal aspects on spin crossover single crystals by optical microscopy [5–12]. These studies have allowed to monitor a HS:LS transformation front upon the spin crossover transition and to follow the spatio-temporal features of the HS:LS interface. Such results have evidenced the important role of the mechanical stresses on the front shape and on the nucleation and growth process as well as on the interface propagation. In spin crossover solids, the lattice strain, originating from the molecular volume expansion or decompression overall the crystal, gives rise to long-range interactions, a fact which was first pointed out by Ohnishi and Sugano [13]. Therefore, a volume change of a few molecules, uniformly distributed in the crystal, leads to an internal pressure which reflects at the surface of the crystal (due to the finite volume), called the image pressure [14,15]. This pressure effectively acts on all molecules of the crystal (independent of distances) with the same strength. The contribution of the elastic interactions has been studied in detail both theoretically [16–26] and experimentally by measuring the elastic constants by Brillouin spectroscopy [27] and the strain tensors through temperature dependent x-ray diffraction [28]. From the experimental point of view, the spatiotemporal properties of SC solids have been first revealed only recently through extensive optical microscopy investigations on cooperative and noncooperative single crystals [6,7,9,12].

Most of the experimental observations of optical microscopy demonstrated that the thermally induced SC transition appears first around some defect and then propagates along a well stable direction with the presence of a front transformation characterized by a stable orientation and a well-defined shape. Several elasto-electronic models [21,29,30], including the system's volume change at the transition, have been designed to describe this phenomenon and some of them succeeded to capture a large part of the problem. For example, they well reproduce the existence of a single domain nucleation and growth as well as the stabilization of the front transformation by the elastic long-range interactions, induced by the volume change of the system. Unfortunately, these models have no analytical solutions and their investigations require the use of molecular dynamics (MD) or Monte Carlo (MC) simulations (some of them combine both techniques). It is worth noticing that the experimental values of the velocity of the front transformation are around some μm/s, while both simulation techniques previously quoted do not allow one to obtain realistic time scales. For example, MD is in the picosecond time scale and that of MC simulations is purely phenomenological and has no direct relation with the experimental time. So, these models, although very instructive, have serious limitations when we want to compare quantitatively the theoretical results with the experimental data. In addition, they are limited in size because they are

---

[*] kbo@physique.uvsq.fr

highly time consuming. On the other hand, at the macroscopic scale of the optical microscopy observations (performed on crystals of a few hundred microns in size with a resolution comprised between 0.5 μm at 1 μm), the volume changes are hardly visible and only spin state changes through the thermochromism of the material are revealed.

In this work, we propose an alternative type of model allowing one to describe the domain formation and propagation during the spin crossover transition. Here, for the sake of simplicity we do not consider the volume changes of the solid (an extension including this effect is in progress). Our model, however, uses realistic time scales and then allows quantitative comparison with the experimental results. We show in fact that the spin crossover problem is similar to that of a reaction diffusion problem, and thus can be described by a RDE, which was widely used in literature to describe pattern formation in systems involving short-ranged activation phenomena and long-range inhibition, like in the case of Hydra [31], or in population models in the Fisher-Kolmogorov equation [32,33], and in susceptible-infected-removed (SIR) models for the spread of infectious diseases such as AIDS or rabies [34]. Pushing the comparison further, flames [35] in exothermic combustion systems are also reaction diffusion processes. These models are known to give rise to traveling waves of composition during the conversion of the system from a metastable (or unstable) to a stable state. The manuscript is organized as follows: Sec. II is devoted to the presentation of the model and to the derivation of the spatiotemporal equations of motion; in Sec. III we discuss the results of the pattern formation and in Sec. IV we conclude.

II. DERIVATION OF THE REACTION DIFFUSION EQUATION

To introduce the reaction diffusion equation allowing one to study the spatiotemporal properties of spin crossover solids, we first briefly recall the basic aspects of the model from which we built up the present approach. As already widely discussed in the literature, the spin crossover transition can be described in a simple way using Ising-like models [36,37] for which we recall the Hamiltonian,

$$\mathcal{H} = -J\sum_{\langle i,j\rangle} s_i s_j + \sum_i \left(\Delta - \frac{kT}{2}\ln g\right) s_i. \tag{1}$$

In (1), $J > 0$ is the intermolecular "ferromagneticlike" coupling between spin crossover molecules, and s is the fictitious spin with eigenvalues $+1$, -1, associated with the two spin states HS and LS, respectively. Δ is the ligand field splitting, i.e., the energy difference $E(\mathrm{HS}) - E(\mathrm{LS})$ of isolated molecules, g the degeneracy ratio between the HS and LS states, k is the Boltzmann constant, and T is the temperature. Let us denote by $m = \langle s\rangle$ the average value of the magnetization, which connects to HS fraction, n_{HS} through $n_{\mathrm{HS}} = (1+m)/2$. It is straightforward to demonstrate that the self-consistent equation giving the temperature dependence of the magnetization (or the HS fraction), in the mean-field approach, is given by

$$m = \tanh\beta\,(Jm - \Delta_{\mathrm{eff}}), \tag{2}$$

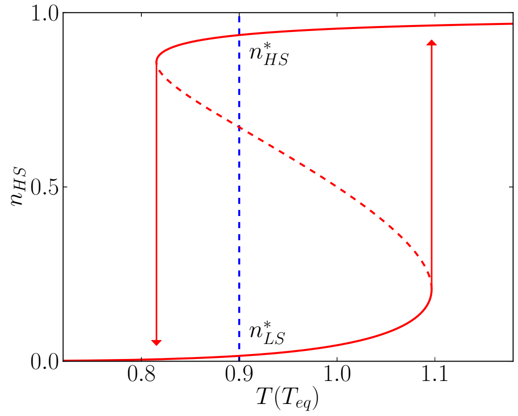

FIG. 1. (Color online) HS fraction vs reduced temperature T/T_{eq} showing the mean-field thermal hysteresis associated with the spin transition, in which we perform the dynamical studies. Dashed blue vertical line represents the temperature of simulation in Sec. III and n^*_{HS} and n^*_{LS} are solutions of Eq. (2). The two arrows indicate the limiting temperatures, T_{down} and T_{up} of the mean-field thermal hysteresis.

where $\Delta_{\mathrm{eff}} = \Delta - \frac{kT}{2}\ln g$ plays the role of a temperature-dependent effective "field." This equation leads to the thermal hysteresis loop presented in Fig. 1, with a transition temperature T_{eq}, given by $T_{\mathrm{eq}} = \frac{2\Delta}{k\ln g}$. The corresponding homogeneous mean-field free energy is easily derived as $\mathcal{F}^{\mathrm{hom}} = \frac{1}{2}Jm^2 - kT\ln[2\cosh\beta(Jm - \Delta + \frac{kT}{2}\ln g)]$.

A. Nonequilibrium properties: the reaction diffusion equation

The nonequilibrium properties of the Hamiltonian (1) have been studied mostly in the homogeneous case [37] in the frame of the master equation formalism [38,39] solved in the mean-field approximation. Three types of dynamics have been investigated, based on Arrhenius transition rates, and Glauber and Metropolis dynamics. While the former leads to the dynamical potential (a kind of Lyapounov function) representation (see Ref. [37]), the two last dynamics give a nonequilibrium system whose dynamics follows the free-energy landscape. At very low temperature, it was proved that the Arrhenius dynamics was the most adequate to describe the nonlinearities of the relaxation curves of the photoinduced HS state. In contrast, at high temperature, the free-energy dynamics becomes also relevant. Since we are interested in the thermally induced hysteresis loop region, we chose to use a free-energy dynamics. Then, the macroscopic equation of motion of the HS fraction writes

$$\frac{\partial m}{\partial t} = -\Gamma\frac{\partial\mathcal{F}^{\mathrm{hom}}}{\partial m} = -\Gamma J[m - \tanh\beta(Jm - \Delta_{\mathrm{eff}})], \tag{3}$$

where Γ is a frequency factor fixing the time scale which can be temperature dependent and $\mathcal{F}^{\mathrm{hom}}$ is the homogeneous *free energy*, whose expression is given above and from which we derived the right-hand side of Eq. (3). At infinite time, we have $\frac{\partial m}{\partial t} = 0$, and the stationary state of (3) leads to find out the equilibrium self-consistent equation (2). It is worth noticing that contrary to the macroscopic master equation, based on the dynamical potential approach [37], which uses "realistic" transition rates, related to the frequency of the metal-ligand stretching vibration mode [40], the frequency factor Γ appearing here is clearly a phenomenological parameter, although its value can be determined from experimental relaxation curves in the high-temperature regime. In addition, we should mention that in Eq. (3), the coordination number $z = 4$ (for a square lattice) is absorbed in the interaction parameter J.

In the following, we propose to extend this previous homogeneous mean-field dynamical approach to account for the space dependence of the HS fraction.

Let $n_{\rm HS}(\vec{r},t)$ represents the spatiotemporal dependence of the HS fraction per site. Also let the field $f(\vec{r}) = f^{\rm hom}(n_{\rm HS}(\vec{r}),\vec{\nabla}n_{\rm HS}(\vec{r}))$ be the density ($\mathcal{F}$/volume) of the free energy $\mathcal{F}$ at position $\vec{r}$. The homogeneous density, $f^{\rm hom}(n_{\rm HS}) = f(n_{\rm HS},\vec{\nabla}n_{\rm HS} = 0)$ is the free-energy density in the absence of gradients and is related to the usual homogeneous free energy $\mathcal{F}^{\rm hom}(n_{\rm HS}) = V \times f^{\rm hom}(n_{\rm HS})$, where V is the volume (here the surface) of the system. Following a standard procedure [41–43] (revisited in Sec. I of [44]) allowing one to derive the reaction diffusion equation, we expand $f(n(\vec{r}))$ in successive powers of the gradients [45] assuming an isotropic material, which gives the following relation:

$$f(n_{\rm HS},\vec{\nabla}n_{\rm HS}) = f^{\rm hom}(n_{\rm HS}) + \frac{D}{2}|\vec{\nabla}n_{\rm HS}|^2. \tag{4}$$

There, the density of the homogeneous free energy, $f^{\rm hom}$, tends to narrow the interface region, while the gradient contribution leads to spread the interface region. The constant D is the diffusion constant and is related to the second derivative of the free energy with respect to the gradient components of the HS fraction [44]. The time dependence of the HS fraction including the spatial variations can be derived from the rate change of the total free energy, $\mathcal{F}^{\rm hom}$, with respect to its current order-parameter field. After some mathematical developments and assuming a small change of the order parameter, we arrive at the RDE, which writes

$$\frac{\partial n_{\rm HS}}{\partial t} = -\Gamma\frac{\partial \mathcal{F}^{\rm hom}}{\partial n_{\rm HS}} + D\,\nabla^2 n_{\rm HS}, \tag{5}$$

which becomes when we use the expression of $\frac{\partial \mathcal{F}^{\rm hom}}{\partial n_{\rm HS}}$ given in (3),

$$\begin{aligned}\frac{\partial n_{\rm HS}}{\partial t} &= -\Gamma J[(2n_{\rm HS}-1) - \tanh\beta(J(2n_{\rm HS}-1)-\Delta_{\rm eff})] \\ &\quad + D\,\nabla^2 n_{\rm HS}.\end{aligned} \tag{6}$$

In (6), the "reaction" terms, obviously due to the homogeneous free energy, act locally while the diffusion coefficient plays the role of a rigidity connecting the local cell to the neighbors. It is worth noticing here that the RDE (6) can be also directly obtained from a variational principle, as reported in [46].

III. SPATIOTEMPORAL PROPERTIES AND PATTERN FORMATION INSIDE THE THERMAL HYSTERESIS LOOP

We now investigate the pattern formation of the SC system in the thermal hysteresis loop of Fig. 1, using RDE (6). We considered a rectangularly shaped 2D lattice with a square symmetry (see Fig. 2), with size $L_x \times L_y = 100\,\mu{\rm m} \times 20\,\mu{\rm m}$. The parameter values used in the model, chosen in order to be realistic as much as possible, are $\Delta = 450$ K, $J = 300$ K, $\Gamma = 1/300$ K^{-1}s^{-1}, $\ln(g) \simeq 5$ (entropy change $\simeq 80$ J K^{-1}mol^{-1}). The corresponding transition temperature is then $T_{\rm eq} = \frac{2\Delta}{k\ln g} \approx 180$ K. The diffusion parameter, D (experimentally unknown), is scanned over a large interval, $D(\mu{\rm m}^2/{\rm s}) \in [0:5]$, so as to reach typical experimental values of the front velocity, some μm/s [6,8]. To solve the RDE (6), the system is coarse grained spatially ($dx = dy = 0.1\,\mu$m) and temporally ($dt = 10^{-3}$ s). The distance between the cells, 1 μm corresponds more or less to the spatial resolution of optical microscopy. The calculations are performed at constant temperature $T = 0.9 \times T_{\rm eq} = 161.65$ K (see Fig. 1), at which the LS (HS) state is stable (metastable). We set initially the system in the metastable HS state (blue area), in which a small square-shaped (red area) LS domain is inserted at the bottom left corner, to initiate the reaction (see the upper left snapshot of Fig. 2).

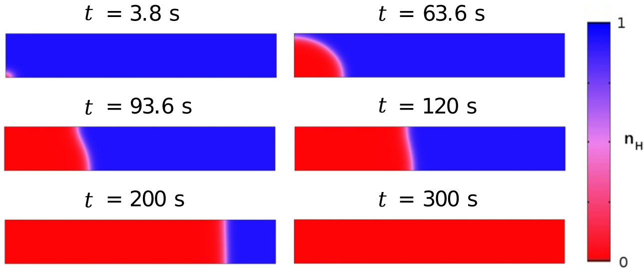

FIG. 2. (Color online) Snapshots of the lattice configurations during the nucleation and growth of the LS state domain inside the thermal hysteresis at temperature $T = 0.9T_{\rm eq}$. The parameter values are given in the text, except $D = 1.0\,\mu{\rm m}^2$/s. Red (blue) area corresponds to LS (HS) state.

A. Structure of the HS:LS interfaces

The resolution of the $L_x \times L_y/(dx \times dy) = 2000$ coupled differential equations arising from the discretization of the lattice is performed by the finite difference method. We illustrate in Fig. 2 some selected snapshots of the system configuration showing the spatial distribution of the HS fraction along the relaxation process at times $t = 3.8, 63.6, 93.6, 120.0, 200.0$, and 300 s. One can see that very quickly after the injection of the square-shaped LS domain, it becomes circular, and this shape is maintained as long as its radius ρ is smaller than the width L_y of the lattice. The circular shape of the interface in this region results form the minimization of its length (the interface energy cost) under the constraint of a contact angle of $\pi/2$, imposed by the open boundary conditions. When ρ exceeds the value $L_y = 20\,\mu$m, the transformed region reaches the border of the lattice, then the shape and the orientation of the interface start to change accordingly. After a while, $t \simeq 15$ s, the interface tends to a stable shape, straight and perpendicular to the lattice side borders ($\rho \to \infty$). It is worth noticing that while these results are new in the spin crossover topic, similar behaviors of nucleation and propagation have been already reported in literature of magnetic materials [47,48], where magnetic domain wall propagation is driven by an applied magnetic field. However, the present situation is much more similar to

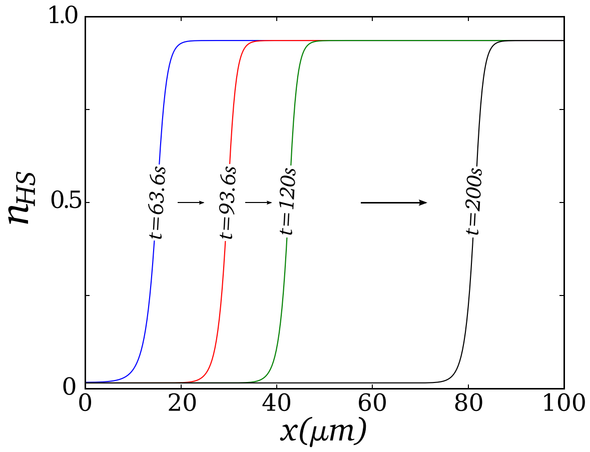

FIG. 3. (Color online) Interface profile along the propagation direction corresponding to the different configurations of Fig. 2. The simulated curves computed using RDE (6) nicely follow Eq. (7), given in the text.

the nucleation and propagation of domains in ferroelectric systems in the vicinity of the thermal instabilities caused by the presence of first-order phase transition. Although, similar to the domain wall propagation in magnetic systems, fundamental differences exist between these two phenomena, since entropic (thermal) effects play an important role in the present case, because we are dealing with a thermally driven first-order phase transition.

B. Study of the flow regime

We now focus on the flow regime, which is characterized by the presence of a straight and stable-shaped interface traveling at constant velocity. The propagation of the transformation along the x axis can be followed by selecting a typical y value and plotting the $n_{\rm HS}(x)$ dependence for different t values. The obtained curves are shown in Fig. 3. They represent propagative solutions of the so-called Kolmogorov equation [33]:

$$n_{\rm HS}(x,t) \simeq \frac{n^*_{\rm HS}+n^*_{\rm LS}}{2} + \frac{n^*_{\rm HS}-n^*_{\rm LS}}{2}\tanh\left(\frac{x-x_0}{\omega}\right), \qquad (7)$$

where $x_0 = vt$ is the position of the interface center, ω the interface width, and $n^*_{\rm HS}$ and $n^*_{\rm LS}$ are solutions of the mean-field self-consistent equation (2).

We followed the interface position as a function of time during the propagation process of Fig. 2. The results are presented in Fig. 4(a), for three selected y values, $y = 1$, $y = N_y/2$, $y = N_y$, corresponding to the bottom, the center, and the top of the lattice, respectively. In all cases, the used value of the diffusion constant, $D = 1.0\,\mu\text{m}^2\,\text{s}^{-1}$ leads at long time, to a constant propagation velocity, $v \simeq 4.5\,\mu\text{m/s}$, of the HS:LS interface; a result which is consistent with the available experimental data [5–12]. Furthermore, an inspection of the simulated interface profiles of Fig. 3, leads to width value, $\omega \simeq 10\,\mu\text{m}$, which is also in quite good agreement with optical microscopy observations [6–8]. A detailed comparison to the experimental data will be presented in the next section.

We have also studied the dependence of the interface velocity and width upon the diffusion constant D, and found in both cases that v and ω grow as $\sqrt{D}$ [44], a result which was already reported in literature [46], where scaling analysis showed that the interface width scales as $\sqrt{D}$ and the interface speed is proportional to this width.

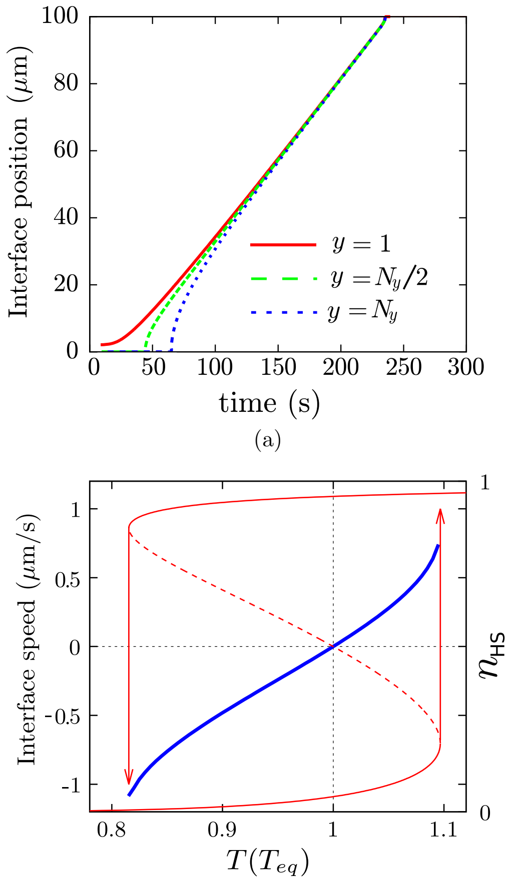

(a)

(b)

FIG. 4. (Color online) (a) Time dependence of the HS:LS interface position along the propagation direction (x axis) for different y values. (b) HS:LS interface velocity (blue curve), in the flow regime vs reduced temperature $T/T_{\rm eq}$ inside the thermal hysteresis of Fig. 1 which is represented here (red curve). Remark the linear character of the interface speed with temperature and its particular value ($v = 0$) at the transition temperature (the Maxwell point).

1. *The driving force of the interface propagation*

Next, we studied the temperature dependence of the front speed inside the hysteresis loop. The results are presented in Fig. 4(b) and show that the interface velocity behaves linearly in the transition temperature region and increases when approaching the upper and lower temperatures of the hysteresis loop, which are the limiting temperatures of metastability of the LS and HS phases, respectively. To identify, much more precisely, the driving force and the relevant parameters at the origin of the interface motion, we expanded the expression of the homogeneous free energy in powers of the HS fraction around the equilibrium temperature and we found that the front velocity, $v = \frac{dx_0}{dt}$ obeys the relation,

$$v = \frac{3}{2}k(T - T_{\rm eq})\sqrt{\frac{2D\Gamma}{J}}\ln g, \qquad (8)$$

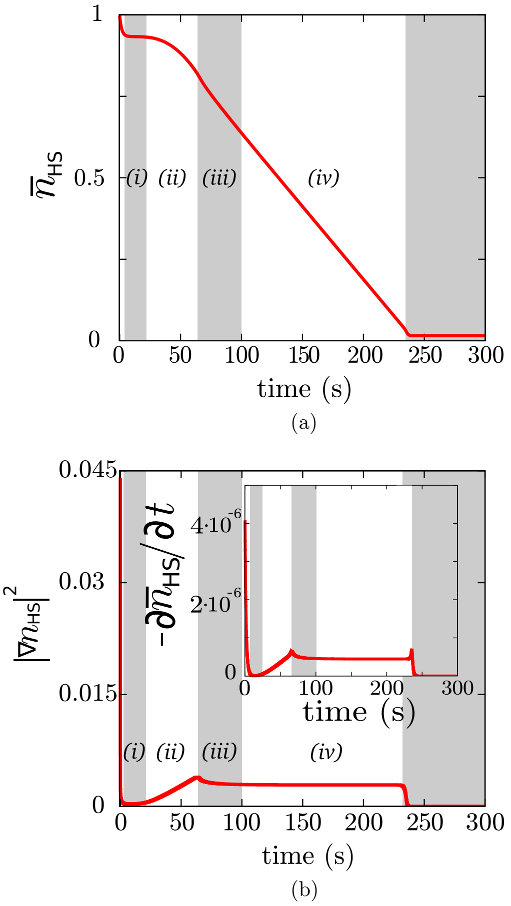

FIG. 5. (Color online) (a) Time dependence of the average HS value corresponding to the interface propagation of Fig. 2. (b) Time dependence of the square of the average gradient of the HS fraction, showing the different regimes involved during the interface propagation. (Inset) Time derivative of HS fraction, $-\frac{\partial n_{HS}}{\partial t}$ vs time. See text for more explanations. The parameter values are those of Fig. 2.

which agrees very well with the numerical results depicted in Fig. 4(b). Equation (8) allows one to identify the driving force of the front motion as due to the effective field, $\Delta_{\text{eff}} = \Delta - kT \ln g = k \ln g (T_{\text{eq}} - T)$, which can be expressed as the "distance" between the system's temperature and the transition temperature.

C. Edge effects and transient regimes

The edges of the system play a major role during the propagation process. First of all, they govern the orientation of the interface in the flow regime, through the geometric condition of a border-interface right angle, in the present case of free boundary conditions and high-symmetry lattice. This condition would not be obeyed in the case of lower-symmetry systems. In addition, the beginning and the end of the process are obviously impacted by edge effects associated with the vicinity to the extremities of the system. This is conveniently visualized by plotting the spatially averaged HS fraction as a function of time [see Fig. 5(a)]. Four successive regimes are easily identified : (i) onset of the front shape, followed by (ii) the propagation of a circular front until it reaches the top border, (iii) reshaping towards a linear shape, and (iv) flow regime at constant propagation velocity. In the latter, the total averaged HS fraction behaves linearly in time. Indeed, in this region where the interface's orientation is stable, one can easily understand that the HS fraction writes, $n_{HS} \propto 1 - x_0/L_x$, where x_0 is the position of the front and L_x is the lattice length [see Fig. 5(a)]. On the other hand, while the quoted four regimes are hardly seen in the relaxation curve of the average HS fraction, they appear quite clearly in Fig. 5(b) (and inset), where we represent the time dependence of the gradient, $|\vec{\nabla} n_{HS}|$ (the time derivative, $-\frac{\partial n_{HS}}{\partial t}$), of the HS fraction, which is mostly sensitive to the interface region, and then to the interface length evolution. A meticulous inspection of these curves allows one to conclude that (i) the first regime, characterized by a very rapid relaxation due to the onset of the front transformation from the initially injected square shape to circular shape, is located in the time interval $[0 - 20]$ s, while the second step $[20 - 70]$ s corresponds to the propagation of the front along the width of the lattice (that is, the shortest length) towards the nearest surface (here, border). During this process the radius increases until it reaches the value of the lattice's width, which results in an increase of the interface length and consequently that of the associated HS fraction's gradient. In the third step $[70 - 100]$ s, the front's shape transforms from circular to linear due to the edge effects, which decreases the interface length, then the fourth regime $[100 - 240]$ s starts where the interface has a stable orientation and a constant length, leading to a plateau in the behavior of $\|\vec{\nabla} n_{HS}\|$ and $-\frac{\partial n_{HS}}{\partial t}$. In the last regime, the interface feels the surface (the lattice border) and the front shape changes again to circular before disappearing. In this region, the change in the propagation properties is enhanced when the border-front distance becomes of the same order of magnitude as the interface width.

D. Comparison to experiments

To improve the present spatiotemporal model, we compared quantitatively the obtained results with those derived from optical microscopy experiments on the spin crossover sample [$\{\text{Fe(NCSe)(py)}_2\}_2(m\text{-bpypz})$], where py designates pyridine and bpypz designates 3,5-bis(2-pyridyl)-pyrazolate [8]. This material, here abbreviated Fe(NCSe), presents a thermally induced first-order transition between the LS and the HS states accompanied with a hysteresis loop of 10-K width, centered around ~112.6 K, as depicted in Fig. 6. There, we have inserted optical microscopy images of the crystal in the LS, HS and inside the bistable area in which a very well-defined HS:LS interface can be easily identified.

Due to specific anisotropic structural changes upon the spin transition, the HS:LS interface of this system is oriented with an angle of 57^o with respect to the direction of the crystal's length. The absence of elasticity contribution in the present version of the model does not allow one to reproduce this orientation, although extensions in this line are in progress and will be presented in a future work.

We have followed the experimental interface motion inside the hysteresis loop at temperature $T = 115.04$ K where the HS (respectively, LS) state is stable (respectively, metastable),

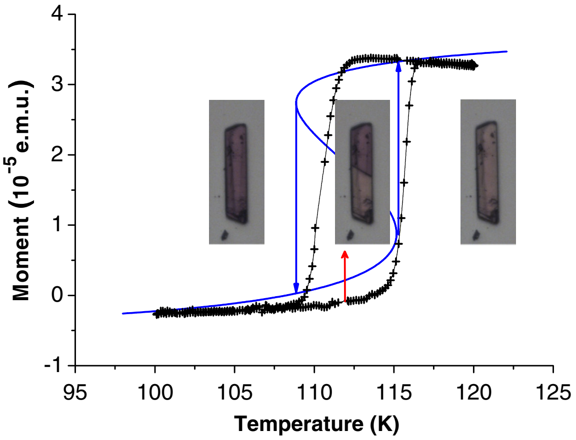

FIG. 6. (Color online) Experimental (black curve) and theoretical (blue curve) thermal hysteresis of the sample Fe(NCSe). The experimental curve results from magnetic measurements on several single crystals and the theoretical curve was calculated within the homogeneous mean-field approach at equilibrium. The three optical microscopy images of the crystal correspond to the three phases, LS (interval 100 – 107.5 K), HS (116 – 120 K), and the coexistence region inside the thermal hysteresis loop.

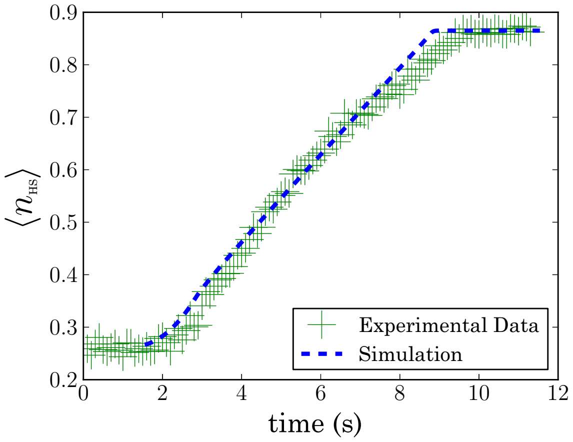

FIG. 7. (Color online) Experimental (crosses) kinetic behavior of the HS fraction during LS to HS transformation of the crystal Fe(NCSe) inside the hysteresis loop at temperature $T = 115.04$ K. The dashed curve is derived from the resolution of RDE. The parameter values are given in the text. An excellent agreement is found between theory and experiment.

above the experimental transition temperature, $T_{\rm eq} = 112.6$ K of the sample. To make a relevant comparison with experiments, we considered a 2D lattice as in the theoretical section, i.e., having a square symmetry and a rectangular shape of size $L_x \times L_y = 100\,\mu\text{m} \times 20\,\mu\text{m}$. The parameter values allowing one to reproduce the experimental thermal hysteresis loop of the HS fraction are $J = 138$ K, $\ln(g) = \ln(150) \simeq 5$ (entropy change $\simeq 80$ J $\text{K}^{-1}\text{mol}^{-1}$), and $2\Delta = T_{\rm eq} \ln(g) \simeq 800$ K. Within these parameters, the self-consistent mean-field Eq. (2) gives the theoretical thermal hysteresis (blue curve) shown in Fig. 6, which reproduces quite well the experimental one. The diffusion parameter and the frequency factor are taken as $D = 16.6\,\mu\text{m}^2/\text{s}$ and $\Gamma \simeq 0.36$ $\text{K}^{-1}\text{s}^{-1}$, respectively. The space and time steps used in the simulations are $dx = dy = 0.1\,\mu$m and $dt = 10^{-4}$ s, respectively. The distance between the cells, taken equal to $0.357\,\mu$m corresponds to the spatial resolution of optical microscopy data presented in this work.

In Fig. 7, we present simultaneously the experimental (crosses) and the theoretical (dashed curve) time dependencies of the HS fraction during the nucleation and propagation process of the front transformation from LS to HS inside the hysteresis loop of Fig. 6. The obtained results clearly indicate a very good agreement between theory and experiments almost overall the time interval. To check the global consistency of our model, we have compared the experimental interface profile (deduced from the spatial dependence of the optical density along the front propagation direction at time $t = 6$ s) with the theoretical predictions, obtained using the same set of parameter values as those leading to the theoretical curve of Fig. 7. The results, summarized in Fig. 8, confirm here also the good quantitative agreement between theory and experiments, as well as the relevance of the model.

Finally, we have also analyzed the local kinetics of the HS fraction on a point inside the crystal. Here, the idea is to follow the time dependence of the HS fraction in a fixed small region of the crystal (one pixel at the scale of optical microscopy measurements, i.e., around $1\,\mu\text{m}^2$) during the front propagation. As long as the front is far from this point, the HS fraction is that of the stationary LS state, i.e., $n_{\rm HS} \simeq 0.3$. When the front comes around the considered point, the HS fraction increases in time until reaching the value of the stationary HS state (i.e., $n_{\rm HS} \simeq 0.9$). The experimental and theoretical results are depicted in Fig. 9 and are in very good agreement with each other. In particular, interesting information arising from this local kinetics analysis concerns the time of local nucleation of the HS fraction, obtained from the width of the curve of Fig. 9, as $\Delta t \simeq 1$ s. This value is an excellent agreement with other experimental lifetime values obtained on different spin crossover compounds using pump probe reflectivity

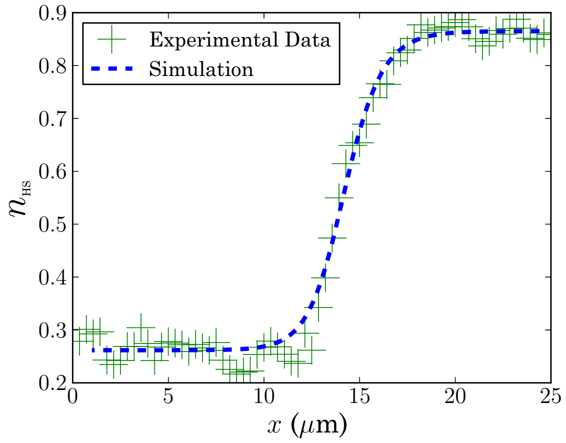

FIG. 8. (Color online) Experimental (crosses) spatial dependence of the HS fraction profile along the propagation direction during the LS to HS transformation of the compound Fe(NCSe). The dashed curve is the theoretical curve, obtained with the same parameter values as those of Fig. 7. The two curves show the spatial cross section of the interface at time $t = 6$ s.

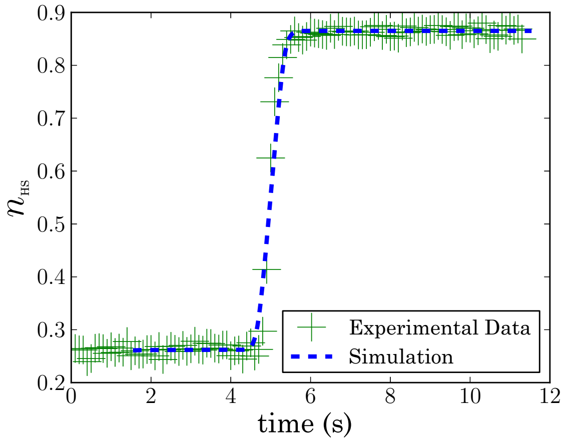

FIG. 9. (Color online) Local kinetics of the LS to HS transformation on a local point of the crystal Fe(NCSe) during the front propagation. Crosses (dashed line) stand for experimental data (theoretical curve). The parameter values of the calculated curve are the same as those of Figs. 7 and 8.

measurements allowing one to monitor the relaxation curves of the HS fraction at different temperatures [49]. On the other hand, it is useful to mention that in recent experimental work, based on optical microscopy investigations on the spin crossover sample $[Fe(btr)_2(NCS)_2].H_2O$ (btr=bis-triazole) [6], a similar plot was obtained and phenomenologically described in terms of a nucleation and growth process, through the Kolmogorov-Johnson-Mehl-Avrami-type law [50], $n_{HS}(t) = C\{1 - \exp[-k(t - t_0)^\gamma]\}$, with an exponent value $\gamma \simeq 2$. For the present sample, it is clearly seen that the hyperbolic tangent law, given in Eq. (7), leads to an excellent agreement with the experimental results. Moreover this good accordance with the experimental data is obtained with the same parameter values as those used for Figs. 7 and 8, which demonstrates the whole consistency of the reaction diffusion model in the description of the spatiotemporal properties of switchable spin crossover solids.

IV. CONCLUSION

We have presented a general description of the interface dynamics at the thermally induced spin transition of spin crossover solids. For that, we have extended the macroscopic homogeneous master equation, describing the relaxation properties of SC solids, by incorporating the spatial dependence of the HS fraction. We found that the general equation of motion accounting for the spatiotemporal properties of SC solids writes as a reaction diffusion equation, where the diffusion phenomenon concerns the spin states. Considering an isotropic system, in which the diffusion constant D is taken as independent of the space directions (as well as temperature and HS fraction), we have calculated the time dependence of the HS fraction inside the thermal hysteresis loop of a spin crossover solid and derived the temperature dependence of the interface speed inside the coexistence region. Four dynamical regimes have been evidenced through the propagation mechanism and their origins have been identified and explained. To check the accuracy of this approach, we performed a comparative analysis between the theoretical predictions and the experimental spatiotemporal data derived from optical microscopy measurements on the spin crossover sample $Fe(NCSe)(py)_2 2(m\text{-}bpypz)]$. We have compared for the same set of theoretical parameter values (i) the time dependence of the spatially averaged HS fraction, (ii) the spatial shape of the interface profile, and (iii) the time evolution of the local kinetics of the HS fraction. An excellent agreement was found for all of these quantities between theory and experiment, which denotes that the present approach is really very efficient and allows one to capture a large part of the spatiotemporal and the front propagation dynamics in spin crossover solids.

This work offers several interesting extensions. Among them, we quote, (i) the inclusion of elastic properties and volume changes; (ii) the description of the spatiotemporal properties in the vicinity of the light-induced instability to investigate the spatiotemporal properties of the light-induced phase separation that we reported several years ago. Three-dimensional extensions of the present model also constitute a nice challenge and target to approach the realistic cases.

ACKNOWLEDGMENTS

The authors acknowledge the Université de Versailles St-Quentin, CNRS, and ANR Agency (BISTA-MAT: ANR-12-BS07-0030-01) for their financial support.

---

[1] In *Topics in Current Chemistry, Spin Crossover in Transition Metal Compounds I–III*, edited by P. Gütlich and H. A. Goodwin (Springer, Heidelberg/Berlin, 2004), pp. 233–235.
[2] C. P. Köhler, R. Jakobi, E. Meissner, L. Wiehl, H. Spiering, and P. Gütlich, J. Phys. Chem. Solids **51**, 239 (1990).
[3] R. Jacobi, H. Spiering, and P. Gütlich, J. Phys. Chem. Solids **53**, 267 (1992).
[4] K. Boukheddaden, J. Linares, E. Codjovi, F. Varret, V. Niel, and J. A. Real, J. Appl. Phys. **93**, 1 (2003).
[5] F. Varret, A. Slimani, K. Boukheddaden, C. Chong, H. Mishra, E. Collet, J. Haasnoot, and S. Pillet, New J. Chem. **35**, 2333 (2011).
[6] A. Slimani, F. Varret, K. Boukheddaden, C. Chong, H. Mishra, J. Haasnoot, and S. Pillet, Phys. Rev. B **84**, 094442 (2011).
[7] C. Chong, A. Slimani, F. Varret, K. Boukheddaden, E. Collet, J. C. Ameline, R. Bronisz, and A. Hauser, Chem. Phys. Lett. **504**, 29 (2011).
[8] A. Slimani, F. Varret, K. Boukheddaden, D. Garrot, H. Oubouchou, and S. Kaizaki, Phys. Rev. Lett. **110**, 087208 (2013).
[9] F. Varret, C. Chong, A. Slimani, D. Garrot, Y. Garcia, and D. Naik Anil, in *Spin-Crossover Materials: Properties and Applications*, 1st ed., edited by Malcolm A. Halcrow (John Wiley and Sons Ltd. Oxford, UK, 2013), Chap. 16.

[10] S. Bedoui, G. Molnár, S. Bonnet, C. Quintero, H. J. Shepherd, W. Nicolazzi, L. Salmon, and A. Bousseksou, Chem. Phys. Lett. **499**, 94 (2010).

[11] S. Bedoui, M. Lopes, W. Nicolazzi, S. Bonnet, S. Zheng, G. Molnár, and A. Bousseksou, Phys. Rev. Lett. **109**, 135702 (2012).

[12] S. Bonnet, G. Molnár, J. S. Costa, M. A. Siegler, A. L. Spek, A. Bousseksou, W. Fu, P. Gamez, and J. Reedijk, Chem. Mater. **21**, 1123 (2009).

[13] S. Ohnishi and S. Sugano, J. Phys. C **14**, 39 (1981).

[14] H. Spiering, K. Boukheddaden, J. Linares, and F. Varret, Phys. Rev. B **70**, 184106 (2004).

[15] K. Boukheddaden, Phys. Rev. B **88**, 134105 (2013).

[16] N. Willenbacher and H. Spiering, J. Phys. C **21**, 1423 (1988).

[17] H. Spiering and N. Willenbacher, J. Phys.: Condens. Matter **1**, 10089 (1989).

[18] T. Nakada, P. A. Rikvold, T. Mori, M. Nishino, and S. Miyashita, Phys. Rev. B **84**, 054433 (2011).

[19] M. Nishino, K. Boukheddaden, Y. Konishi, and S. Miyashita, Phys. Rev. Lett. **98**, 247203 (2007).

[20] M. Nishino, C. Enachescu, S. Miyashita, K. Boukheddaden, and F. Varret, Phys. Rev. B **82**, 020409(R) (2010).

[21] C. Enachescu, L. Stoleriu, A. Stancu, and A. Hauser, Phys. Rev. Lett. **102**, 257204 (2009).

[22] C. Enachescu, M. Nishino, S. Miyashita, L. Stoleriu, A. Stancu, and A. Hauser, Europhys. Lett. **91**, 27003 (2010).

[23] C. Enachescu, M. Nishino, S. Miyashita, L. Stoleriu, and A. Stancu, Phys. Rev. B **86**, 054114 (2012).

[24] M. Nishino, C. Enachescu, S. Miyashita, P. A. Rikvold, K. Boukheddaden, and F. Varret, Sci. Rep. **1**, 162 (2011).

[25] W. Nicolazzi, S. Pillet, and C. Lecomte, Phys. Rev. B **78**, 174401 (2008).

[26] A. Slimani, K. Boukheddaden, F. Varret, H. Oubouchou, M. Nishino, and S. Miyashita, Phys. Rev. B **87**, 014111 (2013).

[27] J. Jung, F. Bruchhäuser, R. Feile, H. Spiering, and P. Gütlich, Z. Phys. B **100**, 517 (1996).

[28] L. Wiehl, H. Spiering, P. Gütlich, and K. Knorr, J. Appl. Cryst. **23**, 151 (1990).

[29] M. Nishino and S. Miyashita, Phys. Rev. B **88**, 014108 (2013).

[30] A. Slimani, K. Boukheddaden, F. Varret, H. Oubouchou, M. Nishino, and S. Miyashita, Phys. Rev. B **87**, 014111 (2013).

[31] V. Petrov, Q. Ouyang, and H. H. L. Swinney, Nature (London) **388**, 655 (1997).

[32] R. A. Fisher, Ann. Eug. **7**, 355 (1937).

[33] A. N. Kolmogorov, I. G. Petrovsky, and N. S. Piskunov, Bull Moscow State Univ Ser A: Math and Mech **1**, 1 (1937).

[34] S. Ruan, in *Mathematics for Life Science and Medicine* (Springer, Berlin, 2007), Sec. 1.

[35] J. Stam and E. Fiume, in *Proceedings of the 22nd Annual Conference on Computer Graphics and Interactive Techniques* (ACM, New York, 1995), p. 129.

[36] A. Bousseksou, H. Constant-Machado, and F. Varret, J. Phys. I (France) **5**, 747 (1995).

[37] K. Boukheddaden, I. Shteto, B. Hôo, and François Varret, Phys. Rev. B **62**, 14796 (2000).

[38] R. Glauber, J. Math. Phys. **4**, 294 (1963).

[39] M. Suzuki and R. Kubo, J. Phys. Soc. Jpn. **24**, 51 (1968).

[40] A. Hauser, Comments Inorg. Chem. **17**, 17 (1995).

[41] J. E. Hilliard, *Spindoal Decomposition* (American Society for Metals, Metals Park, 1970).

[42] J. W. Cahn, Acta Metall. **9**, 795 (1961).

[43] J. A. Warren, R. Kobayashi, A. E. Lobovsky, and W. C. Carter, Acta Mater. **51**, 6035 (2003).

[44] See Supplemental Material at http://link.aps.org/supplemental/10.1103/PhysRevB.89.024306 for where are given the detailed mathematical derivation of the RDE and additional information on the mechanism of pattern formation.

[45] J. W. Christian, *The Theory of Transformations in Metals and Alloys*, 3rd ed. (Pergamon Press, Oxford, 2002).

[46] P. M. Chaikin and T. C. Lubensky, in *Principles of Condensed Matter Physics* (Cambridge University Press, Cambridge, 1995), Chap. 1.

[47] Mi-Young Im, Lars Bocklage, Guido Meier, and Peter Fischer, J. Phys.: Condens. Matter **24**, 024203 (2012).

[48] S. Lemerle, J. Ferré, C. Chappert, V. Mathet, T. Giamarchi, and P. Le Doussal, Phys. Rev. Lett. **80**, 849 (1998).

[49] J. Degert, N. Lascoux, S. Montant, S. Létard, E. Freysz, G. Chastanet, and J. F. Létard, Chem. Phys. Lett. **415**, 206 (2005).

[50] M. Avrami, J. Chem. Phys. **7**, 1103 (1939).